Proc Indian Natn Sci Acad **80** No. 1 March 2014 pp. 55-75

Review Article

The Way from Today's Materials to New Kinds of Amorphous Solids: Nano-Glasses[+]

H GLEITER*
Institute of Nanotechnology, Karlsruhe Institute of Technology, P.O 3640, 76021 Karlsruhe, Germany and *Nanjing University of Science and Technology, Herbert Gleiter Institute of Nanoscience, Building 340, Nanjing, Jiangsu 2 10094, P R China*

(Received 29 June 2013; Accepted 27 August 2013)

This review discusses the preparation, the atomic structure and the properties of new kinds of nanometer structured solids that consist either totally or partially of non-crystalline components.

In the first part solid materials will be considered that are assembled of nanometer-sized glassy regions connected by glass-glass interfaces (called nano-glasses). The atomic and electronic structure of these nano-glasses (and hence all their structure dependent properties) differ from the ones of today's glasses (same chemical compositions) without glass-glass interfaces. In fact, nano-glasses may open the door to new technologies because they permit - for the first time - to produce non-crystalline materials with controllable defect microstructures and/or chemical microstructures resulting in new kinds of non-crystalline materials with new properties. The control of properties by varying the defect/chemical microstructure was limited so far to crystalline materials and it is the main reason why most present technologies utilize crystalline materials.

In the second part materials will be discussed with nanometer-sized gas or liquid filled pores (nano-porous materials). Their properties are controlled by the high density (~10^{15} mm^{-3}) of solid/liquid or solid/gas interfaces which can be tuned reversibly e.g. by applying an external voltage between an aqueous electrolyte in the pores and a nano-porous material. Due to the high density of these interfaces, the entire nano-porous material actslike a structurally homogeneous body andbecomes a solid of macroscopic dimensions with tunable mechanical, electric, magnetic etc. properties.

Key Words: Nano-Structured Materials; New Non-Crystalline Structures; Amorphous Solids; Nano-Glasses; Nano-Porous Materials; Materials with Tunable Properties

1. Introduction and Basic Concept

The majority of materials that are used by mankind since the early days of the neolithicum (up to 100 000 years ago) up to now are crystalline materials. The oldest known examples are granite and quartz used for producing stone age tools. More recent examples are light weight metals (e.g. Al), semiconductors (e.g. Si), materials with high strength (e.g. steels), superconductors, ferroelectrics, special ferromagnetic materials etc.

The main reason for the preference of crystalline materials is the fact that one can control their properties by modifying their *defect microstructure* and/ or their *chemical microstructure*. Fig. 1 displays the remarkable enhancement of the diffusivity of Cu, Ni, Pd if we introduce a high density of incoherent interfaces into the corresponding single crystals so that nano-crystalline Cu, Ni, Pd result (Wuerschum *et al*. 1997). The modification of the properties of materials by varying their chemical microstructure is displayed in Fig. 2 by means of the work hardening

**Author for Correspondence: E-mail:herbert.gleiter@kit.edu; birgit.limmer@kit.edu*
[+]2012 Edward DeMille Campbell Memorial Lecture of ASM International. This lecture was delivered during the 2012 Materials Science and Technology Conference and Exhibition, October 7-11, 2012, Pittsburgh, PA, USA

of an Al-1.6 at % Cu alloy (Kelly and Nicholson 1963). The work hardening changes by about one order of magnitude if the chemical microstructure (at constant chemical composition) is changed from an Al-Cu solid solution to a two-phase material (by an annealing treatment).

Glassy materials (although known since about 11000 years e.g. in the form of obsidian), have not yet been utilized to a similar extent. The most important applications seem to be windows, lenses, optical fibers, amorphous ferromagnets and coatings consisting of polymers or glasses.

The main reason for this less frequent use of glasses is that they are mostly produced by quenching the melt and/or the vapour. Obviously, this approach does not permit to introduce *defects* into the glass that are – for example — similar to grain boundaries (cf. Fig. 3c) or to introduce a *chemical microstructure* similar to the one shown in Fig. 2. As a consequence, one cannot control the properties of today's glasses by the controlled modification of their defect and/or chemical microstructures.

It is the idea of nano-glasses to generate a new kind of glasses that allow us to modify the *defect microstructure* and/or the *chemical microstructure of glasses* in ways comparable to the methods used today for crystalline materials (cf. Figs. 1 and 2). The basic concept of this approach is schematically explained in Fig. 3 by comparing the microstructures of nano-glasses and of nano-crystalline materials. If we consider a melt (Figs 3a and 3e) consisting of one kind of atoms only, we obtain a single crystal (Fig. 3b) if we solidify this melt under conditions close to equilibrium. A nano-crystalline material with a high density of defects in the form of incoherent interfaces is obtained by consolidating nanometer-sized crystals (Fig. 3c). If the consolidated nanometer-sized crystals have different chemical compositions e.g. Ag crystals and Fe crystals (labelled as A and B in Fig. 3d), we obtain a multi-phase nano-crystalline material (Fig. 3d).

It is the idea of nano-glasses (Jing *et al*. 1989; Gleiter 1991, 2008; Weissmuellar *et al*. 1991) to apply the analogous approach to non-crystalline materials. In other words, to apply the consolidation of nanometer-sized glassy clusters in order to generate glasses with a high density of interfaces between adjacent glassy regions with either the same or with different chemical compositions. By consolidating nanometer-sized glassy clusters (Fig. 3g), we generate a non-crystalline solid material that consists of nanometer-sized glassy regions (corresponding to the nanometer-sized crystallites in Fig. 3c) connected by interfaces with an enhanced free volume and different atomic structure relative to the adjacent glassy

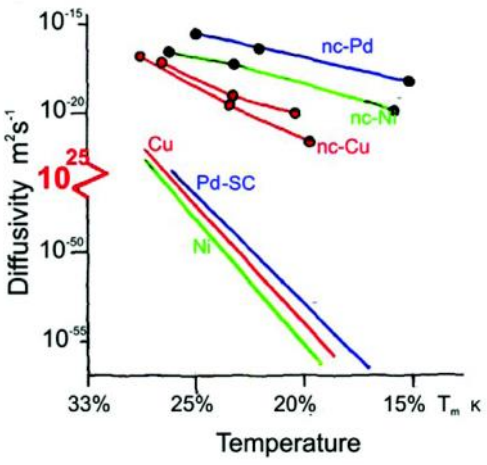

Fig. 1: Comparison of the diffusivities in nano-crystalline (nc) Cu, Ni and Pd in comparison to the diffusivities in single crystals (SC) of Cu, Ni and Pd. T_m is the absolute melting temperature (Wuerschum *et al.* 1997)

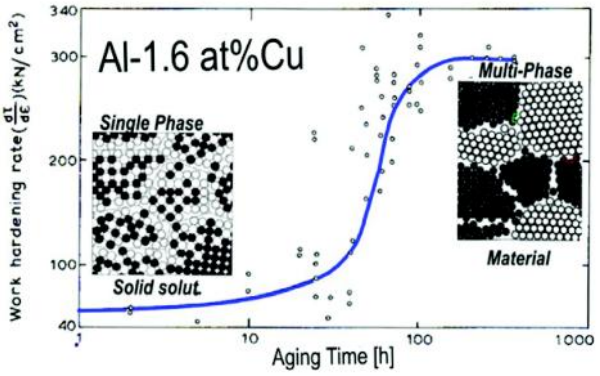

Fig. 2: Work hardening rate of Al-1.6 at % Cu crystals at room temperature after a solution treatment, water quenching, and ageing at 190°C for various times. The strain rate of the deformation process was $3x10^{-4}$ s^{-1}. Initially the specimens were Al-Cu-solid solutions. The aging at 190°C resulted in the formation of a two phase material consisting of precipitates embedded in a crystalline matrix (Kelly and Nicholson 1963)

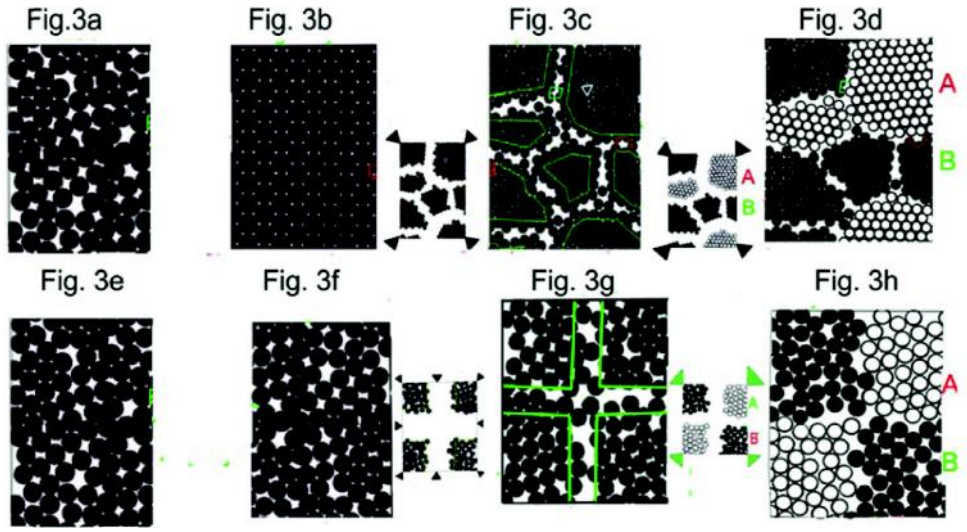

Fig. 3: Figure showing the analogy between the defect and the chemical microstructures of nano-crystalline materials and nano-glasses. The defect microstructure (Fig. 3c) and chemical microstructure (Fig. 3 d) of nano-crystalline materials is compared in Fig. 3g and Fig. 3h with the corresponding defect microstructure (Fig. 3g) and the chemical microstructure (Fig. 3h) of nano-glasses. Fig. 3f shows the structure of a glass that is available today. It results if the melt is rapidly cooled below the glass transition temperature

clusters due to the misfit between the atoms at the surfaces of the glassy clusters similar to the (non-crystalline) atomic structure of the inter-crystalline interfaces displayed in Fig. 3c. Due to the analogy of the nanometer-sized microstructures of both materials (Figs. 3c and 3g), the glass shown in Fig. 3g is called a nano-glass. Again, if we consolidate nanometer-sized glassy clusters of different chemical compositions (Fig. 3h), we obtain a multi-phase nano-glass that is micro-structurally analogous to the multi-phase nano-crystalline material shown in Fig. 3d.

2. Results and Discussion

(a) Nano-Glasses

Production of Nano-Glasses: So far, nano-glasses have been produced in the following three ways:

(b) Inert Gas Condensation

One way to produce nano-glasses, is by means of inert gas condensation (Fig. 4). This production process involves the following two steps [3-6]. During the first step, nanometer-sized glassy clusters are generated by evaporating (or sputtering) the material in an inert gas atmosphere. The resulting clusters are subsequently compacted at pressures of up to 5GPa

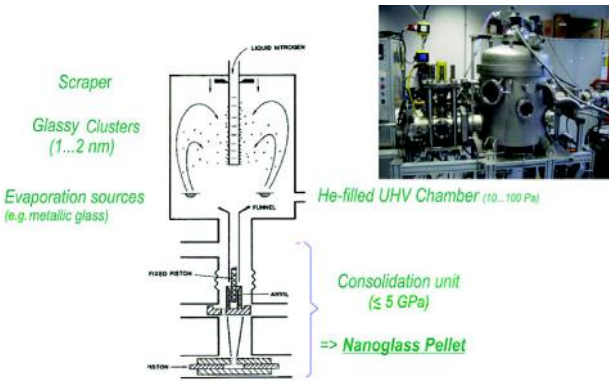

Fig. 4: Production of nano-glasses by consolidation of nanometer-sized glassy clusters that are generated by inert gas condensation [3-6]

into a pellet shaped nano-glass. So far, nano-glasses have been synthesized by inert gas condensation from a variety of alloys: Au-Si, Au-La, Fe-Si, Fe-Sc, La-Si, Pd-Si, Ni-Ti, Ni-Zr, Ti-P (Jing *et al*. 1989; Gleiter 1991, Weissmueller *et al*. 1991; Fang *et al*. 2012).

(c) Magnetron Sputtering

This method (Fig. 5) has been applied so far to Au-based and a Ti-based metallic glasses (Chen *et al*. 2011, 2013). The targets used were mixtures of the alloy elements in the form of powders with a particle

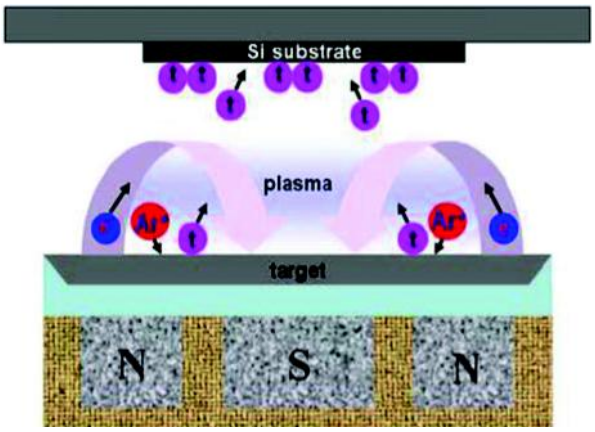

Fig. 5: Synthesis of an Au-based nano-glass by magnetron sputtering (Chen *et al.* 2011)

size of about 100°C. The background gas pressure was lower than 10^{-4} Pa and the working pressure was 0.67 Pa. The nano-glass obtained consisted of glassy regions with an average size of about 30 nm.

(d) Severe Plastic Deformation

Due to the enhanced free volume in shear bands (Li 2002; Shao *et al*. 2012), the average free volume content of a glass was found to increase (Feng *et al*.; Liu *et al*. 2010) with increasing plastic deformation. However, despite of the similarity between the microstructural features of a nano-glass produced by consolidating nanometer-sized glassy spheres and a nano-glass produced by introducing a high density of shear bands, the results of recent studies by molecular dynamics (MD) suggest (cf. the section on Studies by Molecular Dynamics) that the atomic structure of both kinds of nano-glasses may differ. This conclusion seems to be supported by recent results utilizing Moessbauer spectroscopy to characterize the atomic structure of nano-glasses produced by severe plastic deformation and inert gas condensation. The Moessbauer spectra of a ball milled $Fe_{90}Sc_{10}$ glass and of a nano-glass produced by inert gas consolidation with the same chemical composition were noted to be different. Moreover, the introduction of excess free volume into a glassy structure by means of introducing numerous shear bands does not seem to apply to all kinds of glassy materials. In the case of an ionic material ($LiAlSi_2O_6$), severe plastic deformation by ball milling has been applied to modify the structure of the crystalline as well as the glassy form of this material (Kuhn *et al*. 2009). The results obtained suggest that the microstructure of the ball milled $LiAlSi_2O_6$ glass seems to be similar to the one of the nano-crystalline $LiAlSi_2O_6$ (Kuhn *et al*. 2009; Wilkening and Heitjans 2006).

3. Structural Studies

(a) Microscopy, Positron Annihilation Spectroscopy (PAS) and X-ray Diffraction

The granular structure a of $Sc_{75}Fe_{25}$ nano-glass produced by consolidating these $Sc_{75}Fe_{25}$ glassy clusters at a pressure of about 4.5 GPa is displayed in Fig. 6 showing a Scanning Tunneling Microscopy Image (STEM) (White *et al*. 2013) of the polished surface of a nano-glass specimen. The selected area electron diffraction (SAED) pattern (Fig. 7a) evidences (Fang *et al*. 2012) the amorphous structure of the nano-glass. However, the wide angle X-ray diffraction curve (Ghafari *et al*. 2012) of the nano-glass and of a melt-spun glass with the same chemical compositions ($Fe_{90}Sc_{10}$) revealed (Fig. 7b) that the coordination number of nearest neighbour atoms in the range between 0.21nm and 0.31nm was 10.5 for the nano-glass and 11.3 for the melt-spun glass. If

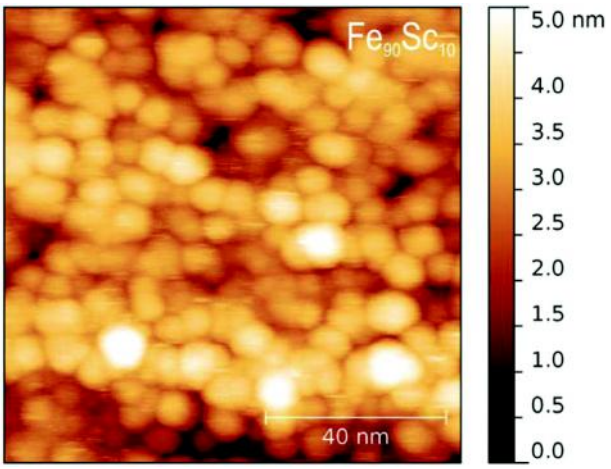

Fig. 6: Constant current Scanning Tunneling Electron Micrograph (STEM) of the polished surface of a $Sc_{75}Fe_{25}$nano-glass specimen. The STEM reveals the granular structure of the $Sc_{75}Fe_{25}$nano-glass produced by consolidating $Sc_{75}Fe_{25}$ glassy clusters by applying a pressure of 4.5 GPa (Witte *et al.* 2013)

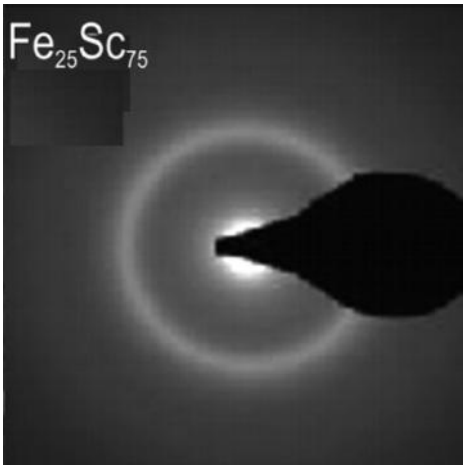

Fig. 7a: Selected electron diffraction pattern of a $Sc_{75}Fe_{25}$nano-glass (Fang *et al.* 2012)

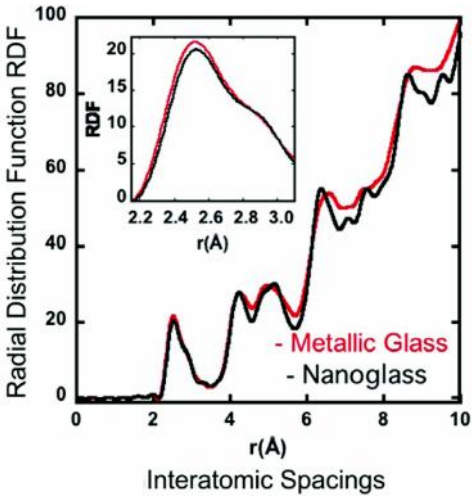

Fig. 7b: Radial distribution functions (RDFs) of a melt-spun metallic glass ($Fe_{90}Sc_{10}$, red curve) and a nano-glass with the same chemical composition (Ghafari *et al.* 2012). The insert displays the RDFs of the melt-spun glass and the nano-glass for interatomic spacings between 0.22 and 0.31 nm in greater detail

the coordination numbers in the reference glass and in the glassy regions of the nano-glass are assumed to be identical, the coordination number in the glass-glass interfaces is found to be 9.1 i.e. reduced by about 20%. (Moessbauer spectroscopy indicated a volume fraction of 35% of glass-glass interfaces in these specimens.) Structural investigations by elemental mapping (Fang *et al*. 2012) was used to obtain information about the local chemical composition of the nano-glass. A composition of approximately $Sc_{85}Fe_{15}$ was found in the interfacial regions of a $Sc_{75}Fe_{25}$nano-glass (Fig. 7a). The compositions inside of the glassy clusters were found to vary between $Sc_{70}Fe_{20}$ and $Sc_{50}Fe_{30}$. In addition, some of the specimens were noted to contain some O or N that may have diffused into the interfaces of the nano-glass when the specimens were exposed to air. Positron Annihilation Spectroscopy (PAS) was applied (Fig. 8) to examine the distribution of the free volume in as-prepared as well as in annealed $Sc_{75}Fe_{25}$nano-glasses (Fang *et al*. 2012). The following two lifetime were found: t_1=169 ps and t_2=285ps in the as-prepared state (Fig. 8). Positron lifetimes in the order of 350-500 ps, as indicators of

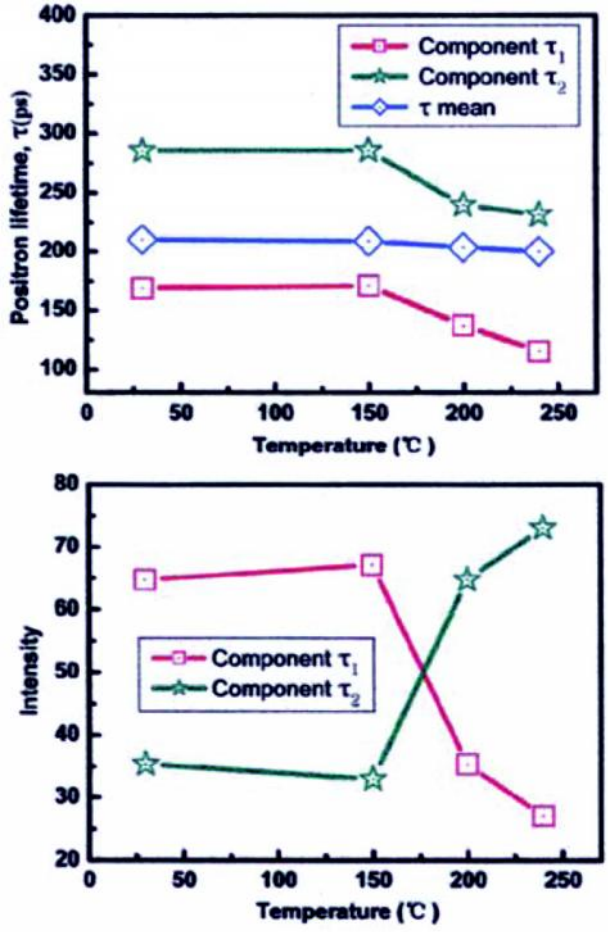

Fig. 8: Upper figure: Positron lifetime of the components t_1 (red line), t_2 (green line)and the mean position lifetime t_m (blue line) ofa $Sc_{75}Fe_{25}$nano-glass. Lower figure: Relative intensities of the same components (t_1 and t_2) in the as-prepared state of the $Sc_{75}Fe_{25}$nano-glass and variation of t_1 and t_2 during annealing (Fang *et al.* 2012)

nano-voids, were not observed. The component $\square_1$=169 ps is comparable to the positron lifetime in melt-spun amorphous ribbons with the same chemical composition. Therefore, the t_1 component was interpreted to originate from the interior of the glassy regions of the nano-glass. The second component (t_2=285 ps) was observed exclusively in the as-consolidated nano-glass. Hence, this component was suggested to originate from the glass-glass interfaces, characterized by an enhanced free volume. According to Fig. 8 (lower figure), the volume fraction of the glass-glass interfaces in the as-prepared $Sc_{75}Fe_{25}$nano-glass was about 65 %. When the $Sc_{75}Fe_{25}$nano-glass was annealed, the intensity of the t_2 component decreased from initially 65 % to about 25 % (Fig. 8). Simultaneously, the intensity of the t_1 component changed from 35% to about 75 % (Fig. 8).

In order to study the microstructure of a $Sc_{75}Fe_{25}$nano-glass, Small Angle X-ray Scattering experiments (SAXS) were applied (Fang *et al*. 2012). The SAXS curves obtained (Fig. 9a) are composed of the following two components: a power-law component (due to fractal fluctuations of the electron density) and a superimposed hump. The superimposed hump indicates that the structure of the nano-glass consists of regions of higher and lower density. The mean diameter of the regions with higher density was obtained to be about 3.0 nm (Fig. 9b). By combining the SAXS (Fig. 9a) and the PAS (Fig. 8) results, one obtains a difference in the electron density of about 17% between the relative densities of the glass-glass interfaces and the glassy regions (i.e. the density difference between the black and gray regions in Fig. 9b). Similarly, a difference in the density between the glass-glass interfaces and the glassy regions of more than 10% has been reported for an Au-based nano-glass (Chan *et al*. 2011).

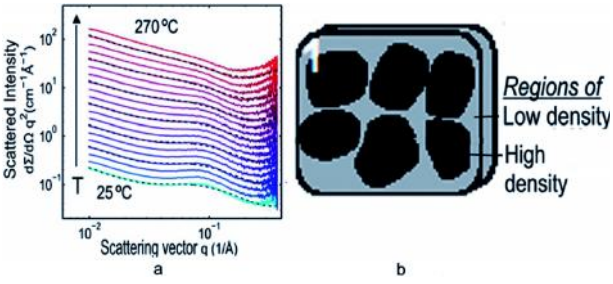

Fig. 9: a: q^2-weighted SAXS curves of a $Sc_{75}Fe_{25}$nano-glass (consolidated at 4.5 GPa) as a function of the annealing temperature. The curves have been shifted vertically for clarity, except for the lowest curve. The scattering vector (q) is defined as 4psin(q)/l, where q is half of the scattering angle and l is the wavelength (Fang *et al*. 2012) and b: Microstructural model of a nano-glass deduced by a Debye-Bueche transformation from the SAXS data shown in Fig. 9a. The nano-glass consists of dense (nanometer-sized, non-crystalline) regions (indicated in dark) embedded in a non-crystalline material with a lower density (gray regions) (Fang *et al*. 2012)

(b) Möessbauer spectroscopy

Fig. 10 shows the Möessbauer spectra and the corresponding quadruple splitting (QS, right side of figure) distributions of a melt-spun $Fe_{72}Si_{18}Fe_{10}$ glass and a nano-glass with the same chemical composition (Jing *et al*. 1989). In comparison to the corresponding melt-spun glass, the QS distribution of the nano-glass consists of two components. The first component coincides with the peak of the melt-spun glass. The second one (at about 0.9 mm s^{-1}, indicated in red in Fig. 10) was observed in the nano-glass only suggesting that it originates from the interfaces between the glassy regions. This interpretation agrees with the observation (Jing *et al*. 1989) that the area under the second peak scales approximately with the volume fraction of the interfaces in the nano-glass

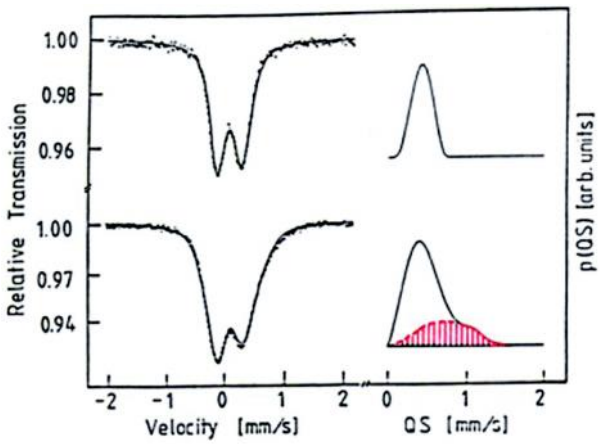

Fig. 10: Moessbauer spectra (left side) and the corresponding Quadrupole Splitting (QS) distribution (p(QS)) of a melt-spun $Pd_{72}Fe_{10}Si_{18}$ metallic glass (upper part of the figure) and of a nano-glass with the same chemical composition generated by consolidating nanometer-sized glassy clusters with an average diameter of 3.6 nm (Jing *et al*. 1989)

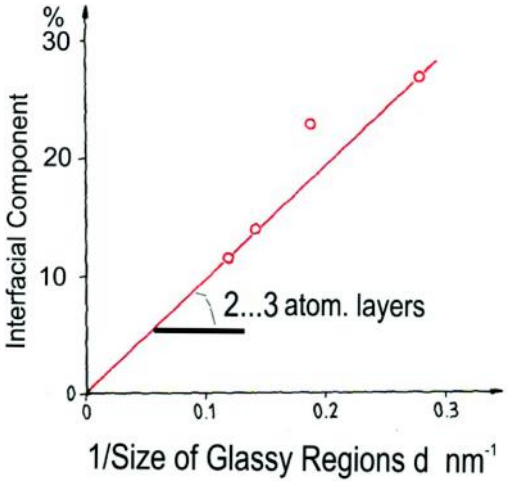

Fig. 11: Relative spectral fraction of the interfacial component versus the invers size of the glassy regions (Jing *et al.* 1989) of the nano-glass shown in Fig. 10. The slope of the curve indicates a width of the boundaries between the glassy regions of the nano-glass of about 2 to 3 atomic layers (Jing *et al.* 1989)

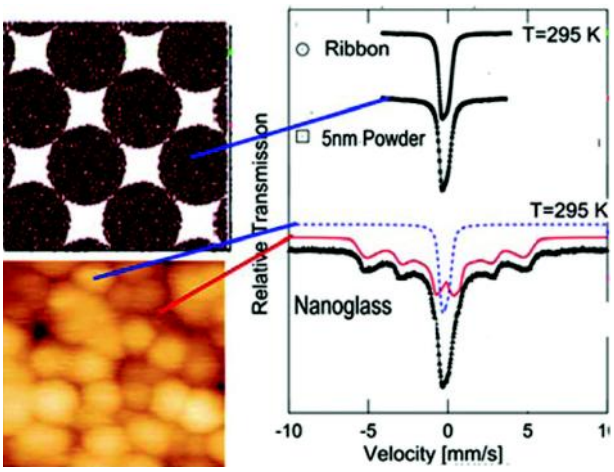

Fig. 12: Möessbauer spectra recorded at 295 K of the melt-spun ribbon,of the 5 nm nano-sphere powder prior to consolidation and of the nano-glass produced by consolidating the 5 nm powder. The unconsolidated powder particles were isolated from one another by coating their surface with an inert gas layer. In all three cases the chemical composition was $Fe_{90}Sc_{10}$. The melt-spun ribbon and the unconsolidated nano-sphere powder exhibit the identical single line spectrum typical for paramagnetic materials (upper right side of Fig. 12). The nano-glass spectrum (lower right side of Fig 12) may be separated in a paramagnetic component (PM, blue line in Fig. 12), with a spectral shape similar to the ribbon (or the powder) and a ferromagnetic (FM, red line in Fig. 12) component. The ferromagnetic component consists of six lines that are a characteristic feature of ferromagnetic materials. The straight red and blue lines indicate the location of the regions in the nano-glass that result in two different components (FM and PM) of the Moessbauer spectrum (Whitte *et al.* 2013)

(Fig. 11). From the slope of the line shown in Fig. 11, the thickness of the interfaces was deduced to be ~0.4 nm, corresponding to about two to three atomic spacings. Hence, the structural model (Fig. 3g) of a nano-glass (consisting on nm-sized glassy regions connected by glass/glass interfaces with a reduced density) seems to agree with the Mössbauer (Fig. 10) as well as with the SAXS (Fig. 9) results reported above.

(c) Electronic Structure of Nano-glasses

The different atomic arrangements in the glass-glass interfaces and in the adjacent glassy regions as well as conceivable interfacial segregation effects seem to result in different electronic structures in both regions. A first indication of the different electronic structure was the observation (Jing *et al*. 1989) that the Mössbauer Isomer Shift (IS) of the interfacial component of PdSiFe-glasses (Fig. 10) was larger than the IS value of the glassy regions indicating a reduced s-electron density in the glass-glass interfaces.A further observation indicating different electronic structures of the glassy and of the interfacial regions of a nano-glass was reported (Whitte *et al*. 2013) for $Fe_{90}Sc_{10}$ glasses. Melt-cooled glassy ribbons of $Fe_{90}Sc_{10}$ and of a nano-glass with the same chemical composition displayed different Moessbauer spectra (Fig. 12). The single line spectra of the ribbon as well as of the isolated nanometer-sized glassy spheres indicate that both are paramagnetic. The spectrum of the consolidated spheres (Fig. 12 lower right side) consists of the following two components.

- A paramagnetic component (indicated in blue in Fig. 12, lower right side) similar to the spectrum of the ribbon or of the isolated $Fe_{90}Sc_{10}$ nanometer-sized clusters (Fig. 12 upper right side) and
- A ferromagnetic component (six-line sub-spectrum: red curve in Fig. 12 lower right).

As the ferromagnetism at ambient temperature is observed only if the $Fe_{90}Sc_{10}$nano-spheres are consolidated (Fig. 12), one is led to conclude that it is the interfacial regions between these consolidated spheres that are ferromagnetic. Ferromagnetism has never been observed in any melt-spun or vapour-deposited amorphous Fe_xSc_{100-x} alloys at ambient temperatures (irrespective of the chemical composition). In Fig. 13 the temperature dependence of the magnetic hyperfine field of the melt-quenched ribbon of a $Fe_{90}Sc_{10}$ glass is compared with the one of the interfacial regions of a $Fe_{90}Sc_{10}$nano-glass (Ghafani unpublished research). As may be seen, the ribbon exhibits the typical spin glass behaviour characterized by a slope of ~1.5 in the Magnetic Hyperfine Field (B_{hf}) vs. temperature (T) plot. This behavior is based on the polarization and coupling of localized 3d electrons. In the case of the interfacial component of the nano-glass, the slope of the B_{hf} vs. T plot is found to be ~2 (Fig. 13). This slope indicates (Ghafari *et al*. 2012; Zukoeski *et al*. 1994; Sakurai *et al*. 1994; Sakai 1992) a dominant contribution of the itinerant electrons to the magnetic coupling in the nano-glass interfaces. The same conclusion is suggested by the magnetic Compton profile of the chemically identical nano-glass (Gafari *et al*. 2012) indicating that the itinerant ferromagnetism of the $Fe_{90}Sc_{10}$nano-glass is based on spin-polarized sp-like itinerant electrons (Ghafari *et al*. 2012; Zukoeski *et al*. 1994; Sakurai *et al*. 1994; Sakai 1992).

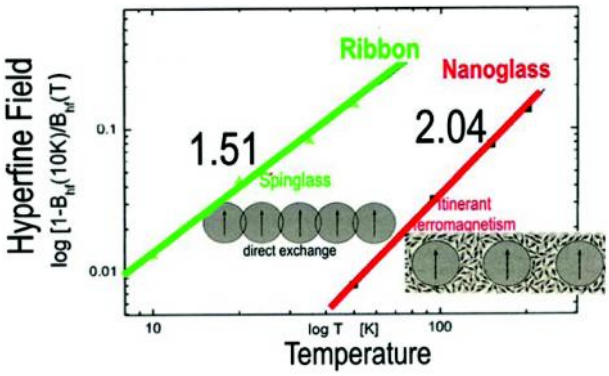

Fig. 13: Diagram displaying the temperature dependence of the measured magnetic hyperfine field (B_{hf}) of a melt-spun ribbon and of a nano-glass both of which have the same chemical composition ($Fe_{90}Sc_{10}$). The $T^{1.51}$ dependence observed for the melt-spun ribbon agrees with spin wave theory that applies to most amorphous metal-metalloid and metal-metal alloys (Gafari *et al*. 2012). In the case of the $Fe_{90}Sc_{10}$nano-glass a temperature dependence of $T^{2.04}$ is observed. A $T^{2.04}$ temperature dependence of the magnetic hyperfine field evidences itinerant ferromagnetism in the nano-glass. Magnetic Compton Scattering performed by using the same specimens indicate that the itinerant ferromagnetism in the nano-glass is caused by negative spin polarized sp-like itinerant electrons (Ghafari *et al*. 2012; Zukoeski *et al*. 1994; Sakurai *et al*. 1994; Sakai 1992)

If the Young's moduli of a $Sc_{75}Fe_{25}$nano-glasses (Chokshi *et al*., Franke *et al*. - unpublished) and $Au_{52}Ag_5Pd_2Cu_{23}Si_{10}Al_6$nano-glasses (Chen *et al*. 2011) are compared with the Young's moduli of the corresponding melt-quenched glassy ribbons, the moduli of the nano-glasses were found (in all cases studied so far) to be higher. As the atomic density in the nano-glass interfaces is reduced in comparison to the density of melt-quenched glasses with the same chemical composition (Fig. 9), the enhancement of the Young's moduli indicates that the interatomic interaction i.e. the electronic structures of the nano-glasses differ from the ones of the corresponding melt-quenched glasses. This conclusion agrees with the results of recent Nuclear Resonant Vibrational Spectroscopy (NRVS) measurements performed at 300K. The mean interatomic force constants in a $Fe_{90}Sc_{10}$ melt spun glass was found to be 138.195 N/m whereas the one in the nano-glass was almost 10% higher (147.965 N/m) (Ghafari unpublished).*

(d) Structural Model of Nano-Glasses

In summary the structural model of metallic nano-glasses that emerges from these observations is displayed in Fig. 14. Nano-glasses are non-crystalline solids consisting of the following two kinds of structurally different regions (somewhat similar to the crystals and the grain boundaries of poly-crystals). Regions (red and yellow in Fig. 14) with the same atomic structure as a glass produced by rapidly quenching the melt. These regions originate from the nanometer-sized glassy clusters that were

*It should be noted that the Young's modulus measurements for the nanoglass exhibited a significantly larger scattering than the ones for the ribbon. One reason may be that the nano-glass has a larger porosity and/or local fluctuations in the chemical compositions. However, the scattering was in all measurements less than the enhancements of the moduli. Moreover, the NRVS data do not depend on porosity.

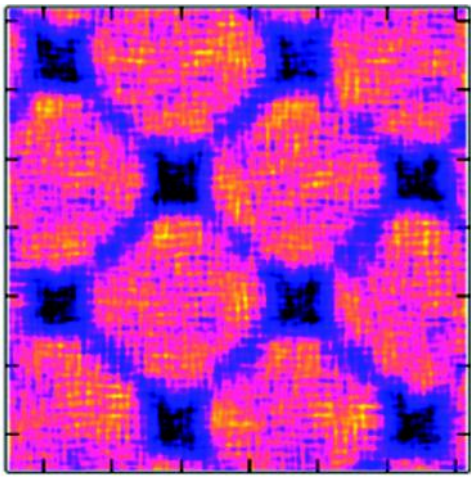

Fig. 14: Proposed model of the structure of a nano-glass. According to the results reported in this paper, nano-glasses consist of the following two kinds of non-crystalline regions. Regions that have the atomic structure of glasses produced by quenching the melt. These regions (indicated in red-yellow color in Fig. 14) result from the consolidated nanometer-sized glassy clusters. The second structural component of nano-glasses (indicated in blue and black in Fig. 14) has a new kind of non-crystalline structure. This new structure is – according to the results reported-characterized (relative to the glassy structure of the chemically identical material indicated in the red-yellow regions of Fig. 14) by a new atomic as well as a new electronic structure. The new atomic structure is characterized by a reduced density, an enhanced spacing between next nearest neighbour atoms and a reduced number of nearest neighbour atoms. The new electronic structure is suggested by the observation of a reduce s-electron density (Moessbauer spectroscopy, Fig. 10), an enhanced Young's modulus and atomic force constant in NRVS, an enhanced Curie temperature and enhanced hyperfine field (Fig. 12) as well as itinerant ferromagnetism instead of a spin glass structure (Fig. 13)

consolidated in order to produce the nano-glass. Between these glassy regions interfacial regions (dark blue in Fig. 14) exist. In these interfacial regions, a new kind of non-crystalline atomic structure (different from the glassy atomic structure in the red and yellow regions) is formed. This new non-crystalline structure is associated with an electronic structure that differs from the one of the corresponding melt quenched glass. The new kind of non-crystalline structure is – according to the results reported above-characterized (relative to the glassy structure in the red yellow regions) by a reduced density, an enhanced spacing between next nearest neighbour atoms and a reduced number of nearest neighbour atoms. The new electronic structure of these interfaces is suggested by the observation of a reduce s-electron density (Moessbauer spectroscopy), an enhanced Young's modulus and atomic force constant in NRVS, an enhanced Curie temperature and enhanced hyperfine field as well as itinerant ferromagnetism (Ghafari *et al*. 2012) instead of a spin glass structure.

(e) Structural Stability of Nano-Glasses

Figs. 15a-g display the results of a Molecular Dynamic (MD) simulation of the microstructural evolution of a three-dimensional nano-glass formed by sintering together glassy spheres (diameter 5 nm) of Ge (Mandelev 2007; Sopu *et al*. 2009). The sintering is caused by applying a hydrostatic pressure of 50 kbar at 300 K.

Figs. 15b-d and e-g present the computed evolution of the atomic structure of this Genano-glass. The figures in the upper row of Fig. 15 (Figs. 15e-g) display the arrangements of the atoms in a thin slab (parallel to the x-y plane, Fig. 15a) with a thickness of 1.5 nm that was cut out of the sintered Genano-glass.

Initially (Fig. 15 e), the fcc arrangement of the glassy Ge spheres (Fig. 15 a) results in a regular arrangement of voids between these spheres (Fig. 15 e). As the sintering process continues (Figs. 15 f and g), the size (volume) of these voids is reduced. In the contact regions between adjacent spheres, glass-glass interfaces are formed. Simultaneously, the widths of these regions of enhanced free volume increases i.e. the interfaces delocalize.

In order to study the structural changes occurring in nano-glasses during annealing in more detail, SAXS/WAXS measurements [14] as a function of temperature and time were performed (Fig. 16). The results displayed in Fig. 16 indicate that when the nano-glass is annealed at temperatures below 230°C (Fig. 16), the width of the glass-glass interfaces increases as a function of temperature. Simultaneously, the relative electron density difference between the glassy and the interfacial

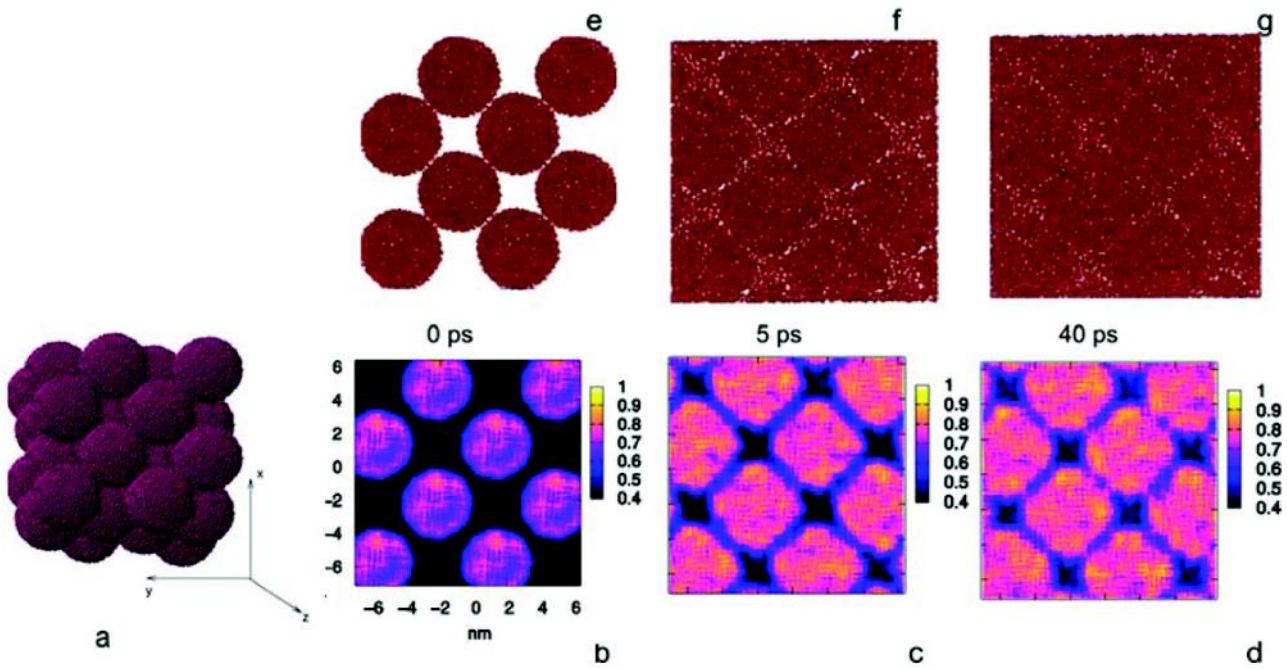

Fig. 15: Molecular Dynamic simulation of the sintering process of a Genano-glass (Sopu *et al*. 2009). The nano-glass is formed by sintering nanometer-sized (5nm diameter) glassy spheres (of Ge) at a pressure of 5 GPa at 300K. Figs. 15(e)-(g) display the atomic structures of the nano-glass by showing the position of the Ge atoms within a thin slab of material cut out of the nano-glass parallel to the x-y-plane, as is indicated in Fig. 15a. The density distribution in this slab of nano-glass during sintering is shown in Figs. 15c and d. The contour plots display the atomic density relative to the density of the melt cooled glass (cf. the density scales on the right side of Figs. 15 b, c and d). It may be seen that the nano-glass consists of a periodic array of dense glassy regions separated by glass-glass interfaces with a reduced density (dark blue color). During annealing, when the sintering process proceeds (Figs. 15b to 15d), the density in the glass-glass interfaces increases. At the same time, these interfaces become wider (Sopu *et al*. 2009)

regions decreases (Fig. 16, left side). This observation agrees with the MD results shown in Figs. 15. However, if the results of the experimental observations (Fig. 16) are compared with the MD results (Figs. 15), the following discrepancy is apparent. The MD results suggest that in the nano-glasses the delocalization process of the glass-glass interfaces occurs – even at relatively low temperatures (e.g. at 300 K) – within a few picoseconds (Figs 15 c and d). However, the experimental observations suggest the delocalization to require - even at 500 K (Fig. 16) – many hours or days. This discrepancy may result from one or both of the following reasons. The first reason may be a chemically inhomogeneous microstructure of the nano-glass as was reported above (Fang *et al*. 2012) for the as-consolidated $Sc_{75}Fe_{25}$nano-glasses. The second reason seems to be that the interatomic interaction potential between the atoms in the glass-glass interfaces differs from the one in the glassy regions due to the different electronic structures in both structural components. (The experimental evidence indicating this difference was discussed above).

4. Properties of Nano-Glasses

(a) Ferromagnetism in FeSc Nano-Glasses

Figure 17 presents the magnetization loops - M

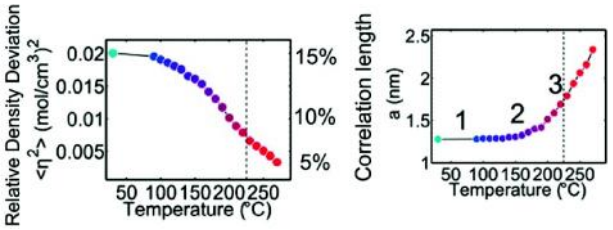

Fig. 16: Results of the Debye-Bueche fit to SAXS data shown in Fig. 9a. The error bars of this fit are smaller than the sizes of the markers. The vertical dashed lines indicate the temperature at which crystallization of the nano-glass was observed to start (Fang *et al*. 2012)

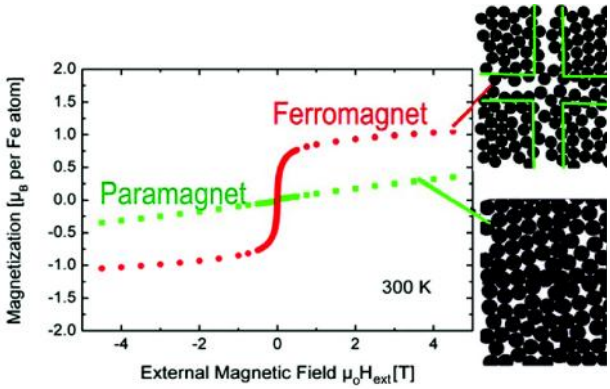

Fig. 17: Magnetization curves (magnetization vs. external magnetic field) of a nano-glass sample (red) and a melt-spun ribbon (green) at 300 K with the same chemical composition ($Fe_{90}Sc_{10}$). The ribbon exhibits paramagnetic behavior, while the nano-glass shows a curve characteristic for ferromagnetic materials with a magnetization of 1 m_B per Fe atom in the applied magnetic field of 4.5 T. The error bars are smaller than the symbols (Whitte *et al.* 2013)

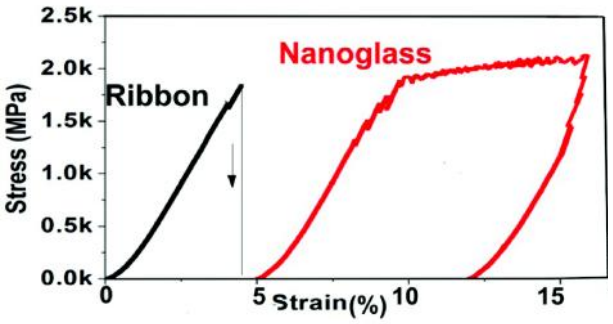

Fig. 18: Computed stress strain curves of a $Sc_{75}Fe_{25}$nano-glass and of a melt-spun ribbon with the same chemical composition (Fang *et al.* 2013)

(magnetization) vs. H (external magnetic field) - of a nano-glass sample and of a melt-spun ribbon having the same chemical composition ($Fe_{90}Sc_{10}$) (Whitte *et al*. 2013). The M vs. H loop - recorded at ambient temperature - evidences that the ribbon is paramagnetic at this temperature, in agreement with the results reported in the literature (Park *et al*. 2006; Cao *et al*. 2010). In contrast, the magnetization curve of the $Fe_{90}Sc_{10}$nano-glass indicates that it is ferromagnetic and it exhibits an average magnetization of about 1.05ºC B per Fe atom.

As has been discussed above, the origin of this ferromagnetism seems to be the different atomic as well as electronic structures of the glassy regions and the interfaces between them.

5. Plastic Deformation of Nano-Glasses

(a) Experimental Observations

By using micro-compression experiments (Fang *et al*. 2013), the deformation behaviour of the following two kinds of glasses were investigated: (1) a melt-quenched ribbon of a $Sc_{75}Fe_{25}$ metallic glass and (2) an as-prepared $Sc_{75}Fe_{25}$ nano-glass. The stress strain plots of these two glasses are displayed in Fig. 18. As may be seen from Fig. 18, the glassy ribbon exhibits brittle fracture (at stresses between about 1900 and 2200 MPa) at a strain of about 5%. The plastic deformation after fracture was less than 1%. The mechanical properties of the glassy ribbon differed significantly from the plastic deformation observed for the corresponding $Sc_{75}Fe_{25}$ nano-glass, as may be seen from Fig. 18. The $Sc_{75}Fe_{25}$ nano-glass (in the as prepared state) was found to yield at a stress of about 1250 MPa. Beyond the yield point, the nano-glass exhibited extensive plastic flow up to about 15%. The fracture stress was about 1950 MPa, which is comparable to the fracture stress of the ribbon. This enhanced ductility may be understood (Albe *et al*. 2012; Sopu *et al*. 2011) in terms of the high density of glass-glass interfaces which may act as nucleation sites for numerous shear bands. In fact, the annealed nano-glass (annealed below T_g) was found (as expected on the basis of this model) to retain a remarkable compressive plasticity with a slightly increased yield strength (~1580 MPa) as well as an increased fracture strength (~2180 MPa). In fact, this interpretation seems to agree with the following observations on the enhanced plasticity of glasses. Lee *et al*. 2007 obtained enhanced plasticity in ZrCuNiAl glasses with a heterogeneous microstructure consisting of hard regions surrounded by soft ones (Wang *et al*. 2009). Other approaches, such as cold rolling (Cheng *et al*. 2008), elasto-static compression (Cao *et al*. 2010; Cheng *et al*. 2008) or nanometer-sized structural heterogeneities (Hofmann 2008; Cheng *et al*. 2008), have also been shown to result in enhanced plasticity.

(b) Studies by Molecular Dynamics (MD)

In order to test these ideas, (Albe *et al*. 2012; Ritter *et al*. 2011; Sopu *et al*. 2011) have investigated by means of MD simulation the plastic deformation of a homogeneous metallic glass ($Cu_{64}Zr_{36}$) and in nano-glasses with the same chemical composition consisting of glassy regions with diameters of either 4 or 10 or 16 nm. The deformation temperature was either 50 K or 300 K. Thestrain rates used were varied between $10^7 s^{-1}$ and $10^9 s^{-1}$.

The MD simulation results obtained suggest that the glass-glass interfaces of a nano-glass may significantly modify the plastic deformation process in comparison to a melt-cooled glass with the same chemical composition. The stress strain curves for the nano-glasses are displayed in Fig. 19a. Their yield stresses were significantly lower than the one of the corresponding melt-cooled glass. This reduction of the yield stress seems to result from the lower nucleation barrier for shear zones at the glass-glass inerfaces in thenano-glass. The locally reduced density in these interfaces seems to be crucial for this effect. As a consequence, the nano-glasses deformed homogeneously (Fig. 19b) in contrast to the corresponding melt-cooled glass (labelled BMG in Fig. 19b) which exhibited localized deformation in the form of one or a few single shear bands, resulting in a significant stress drop in the stress-strain diagram.

(e) Biocompatibility of Nano-Glasses

Due to their high strength, large elastic limit and excellent corrosion resistance, metallic glasses are considered to be promising biomaterials e.g. for medical implants. One of the most widely used implantable metals, titanium and its alloys have attracted considerable scientific and technological interest due to the intrinsic bioactivity, the high resistance to wear and to corrosion resistance of Ti as well as of many Ti alloys. Thus, substantial efforts were devoted to the development of biocompatible Ti-based bulk metallic glasses (BMGs) (Linde 1966; Ma 2003; Hauser 1975; Nastasi *et al*. 1985).

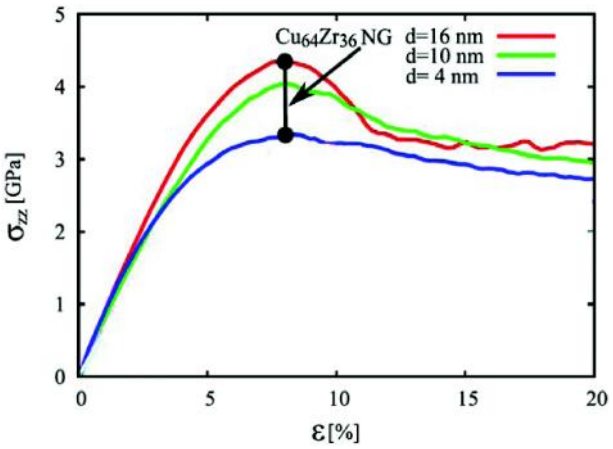

Fig. 19a: Calculated stress-strain curves for $Cu_{64}Zr_{36}$nano-glasses with glassy regions with diameters of 4, 10 and 16 nm (Albe *et al*. 2012; Ritter *et al*. 2011; Sopy *et al*. 2011)

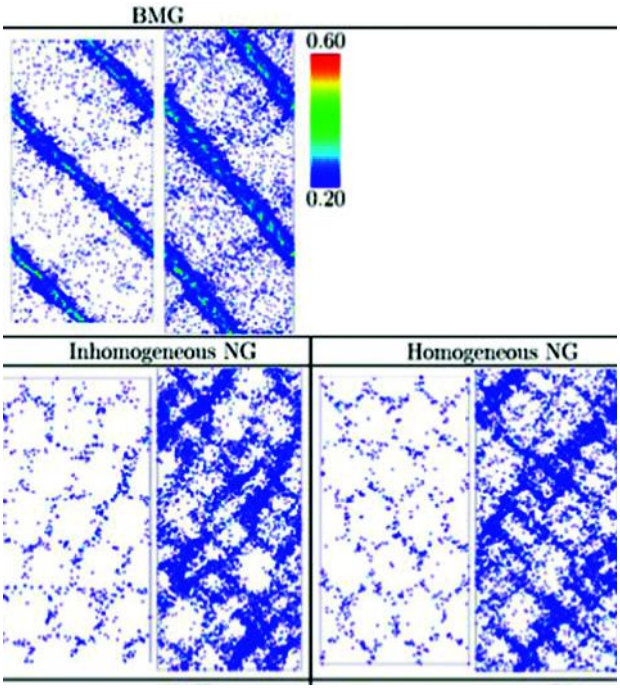

Fig. 19b: Local atomic shear strain for a chemically inhomogeneous (Cu-enriched interfaces) and a chemically homogenous $Cu_{64}Zr_{36}$ nano-glasses (lower right and left figures). The upper figure displays the shear distribution in a metallic glass (labeled BMG) with the same chemical composition (Albe *et al*. 2012; Ritter *et al*. 2011; Sopy *et al*. 2011)

However, without Ni - which is toxic to the human body - Ti-based alloys generally exhibit a lower glass-forming ability (Oak *et al*. 2007; Morrison *et al*. 2007, Qin *et al*. 2007) than the other metal-based BMGs, for example, Zr-based, Cu-based or Fe-based alloys.

On the other hand, it is known that the cellular response to materials is significantly influenced by the microstructure of the implanted materials, their surface roughness, their surface topography and their chemical composition. Therefore, the ability to tailor the microstructures as well as the surface structures of biomaterials by means of nano-glasses may pave the way for designing new glassy materials with improved biocompatibility.

In order to study (Chen *et al*. 2013) the effect of the nano-scale microstructure of nano-glasses on the bioactivity, hierarchically structured layers of $Ti_{34}Zr_{14}Cu_{22}Pd_{30}$ metallic nano-glass were created by magnetron sputtering on different substrates. In order to evaluate the cell proliferation on the surfaces of these materials, ten thousand osteoblasts were seeded on the free surface of either a $Ti_{34}Zr_{14}Cu_{22}Pd_{30}$ metallic nano-glass or on the free surface of two metallic glass ribbons (same chemical composition). As is shown in Fig. 20, the cell density on the surface of the $Ti_{34}Zr_{14}Cu_{22}Pd_{30}$ nano-glass was about fifteen times higher than that on the surface of the corresponding melt-spun ribbon after 7 days. This high level of cell proliferation does not seem to be caused primarily by the surface roughness of the $Ti_{34}Zr_{14}Cu_{22}Pd_{30}$ nano-glass. Both sides of the $Ti_{34}Zr_{14}Cu_{22}Pd_{30}$ glassy ribbons had a roughness that was comparable to the one of the $Ti_{34}Zr_{14}Cu_{22}Pd_{30}$ nano-glass. Despite of the comparable roughnesses,

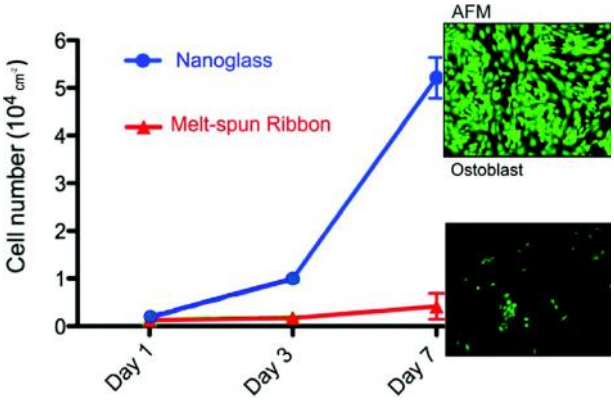

Fig. 20: Cell proliferation at the surface of a melt-spun ribbon and at the surface of a nano-glass with the same chemical composition ($Ti_{34}Zr_{14}Cu_{22}Pd_{30}$). The micrographs on the right side display the density of the osteoblasts (green color) on the surfaces of both materials after a growth time of 7 days (Chen *et al.* 2013)

the ribbons displayed a lower bioactivity than both, the nano-glass as well as a Ti control specimen. The significance of nanometer-sized structure of the surface of nano-glasses agrees with the results of recent studies (Arnold *et al*. 2004; Haung *et al*. 2009; Selhuber-Unkel *et al*. 2010) indicating that the spatial patterning of biochemical cues controls several cellular processes such as spreading, adhesion, migration and proliferationof cells. In fact, these studies indicate that the lateral spacing of individual integrin receptor-ligand bonds determines the strength of cellular adhesion. This seems to be so because integrin clustering and adhesion induced arginine-glycine-aspatic acid (RGD) ligands depend on the local order of the ligand arrangement on the substrate if the average ligand spacing is above 70 nm. Adhesion is "turned off" by RGD patterning above 70 nm and "turned on" below this spacing.

(d) Catalytic Properties

Organosilanols are utilized as versatile building blocks for silicon-based polymer materials (Nagendran 2004; Murugaval 2004), as well as coupling partners in metal-catalyzed coupling reactions (Denmark and Sweis; 2004; Hirabayashi *et al*. 1998; Denmark and Wehrli 2000). As a consequence, methods for removing silanes by an oxidation process with water is attractive from an environmental viewpoint. This oxidation process - summarized in eqn. (1) - should be catalyzed by a heterogeneous catalyst because the catalyst is reusable and the co-product of this oxidation process would be non-polluting hydrogen gas (Mitsudome 2008; Chauhan *et al*. 2009; Mitsudome *et al*. 2009; Yang and Nieh 2007; Sond *et al*. 2010). The $Au_{52}Ag_5Pd_2Cu_{25}Si_{10}Al_6$ nano-glass (called Au-based NGMG in equation 1) was noted (Chen *et al*. 2011) to exhibit a high catalytic activity.

$$\text{(1) } PhMe_2Si\text{-}H + H_2O \xrightarrow[\text{Acetone 300K 24h}]{\text{Au-based NGMG}} PhMe2Si\text{-}OH + H_2$$

In fact, when dimethylphenylsilane was heated with H_2O in the presence of $Au_{52}Ag_5Pd_2Cu_{25}Si_{10}Al_6$ nano-glass, the yield of the reaction (after 24 h at 20°C) catalyzed by $Au_{52}Ag_5Pd_2Cu_{25}Si_{10}Al_6$ nano-

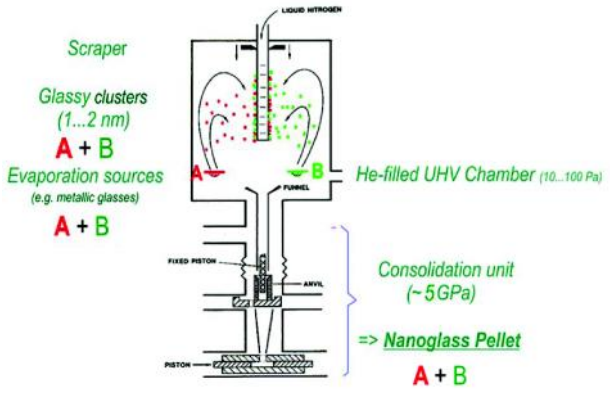

Fig. 21: Production of multi-phase nano-glasses by the consolidation of glassy clusters with different chemical compositions (A and B in Fig. 21). The clusters are generated by evaporating both components simultaneously in an inert gas atmosphere. The resulting clusters of A and B are subsequently collected at the surface of a cold finger (Gleiter 2008). In order to avoid the formation of aggregates of A or B clusters in the inert gas (on the way of the clusters to the cold finger), the evaporation sources for A and B have to be located next to one another (Jing *et al.* 1989; Gleiter 1991; Weissmueller *et al.* 1991; Gleiter 2008)

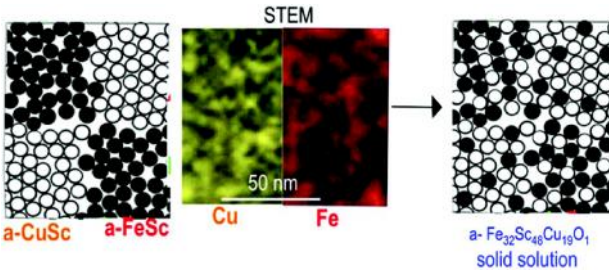

Fig. 22: Structure of a two-phase nano-glass consisting of FeSc and $Cu_{70}Sc_{30}$ glassy clusters (left side). The STEM micrographs in the center of Fig. 22 display the heterogeneous elemental distribution in the two-phases in the nano-glass after preparation. The atomic structure of the glass after annealing is indicated by the drawing on the right side. After annealing of the specimens with a structure as the one shown in the middle, inter-diffusion of Fe, Sc and Cu atoms occurs within the clusters. This interdiffusion result in a chemically homogeneous nano-glass with a composition of $Fe_{32}Sc_{48}Cu_{19}$. This composition evidences that it is possible to generate an amorphous solid solution of Fe-Sc-Cu although these elements are practically immiscible in the crystalline state (Chen *et al.* unpublished)

glass was 93%, whereas only trace amounts of dimethylphenylsilanol were obtained - under the same conditions - with $Au_{52}Ag_5Pd_2Cu_{25}Si_{10}Al_6$ glassy ribbons having flat surfaces.

In order to check if any leaching occurred from the $Au_{52}Ag_5Pd_2Cu_{25}Si_{10}Al_6$ nano-glass, the reaction mixture was filtered to remove the catalyst. In the absence of the catalyst no dimethylphenysilanol was produced indicating that the oxidation process of with water took place exclusively at the surface of the $Au_{52}Ag_5Pd_2Cu_{25}Si_{10}Al_6$ nano-glass catalyst.

6. Multi-Phase Nano-Glasses

(a) Production of Multi-Phase Nano-Glasses

So far multi-phase nanoglasses have been produced by inert gas condensation (IGC) (Gleiter 2008) and by phase separationon a nanometer scale (Mitsudome *et al*. 2008).

The first multi-phase nano-glass produced (Fig. 21) by inert gas condensation (Chen *et al*. (unpublished)) consisted of a mixture of nanometer-sized metallic glassy clusters with the following two compositions: FeSc and $Cu_{70}Sc_{30}$ (Fig. 22). Observations by TEM and WAXS confirmed that the FeSc-$Cu_{70}Sc_{30}$ two-phase nano-glass is indeed a random mixture of both kinds of glassy clusters. Upon annealing below the glass transition temperature an amorphous solid solution of FeScCu was formed (Fig. 22, right side). This result appears remarkable because Fe and Cu are practically immiscible in the crystalline state at similar temperatures.

Although the microstructures of multi-phase nano-crystalline materials and of multi-phase nano-glasses appear similar, there is the following basic difference between both kinds of nano-materials.It is well known from the phase diagrams of numerous alloys that the mutual solubility is in the molten state in most alloy systems much higher than the mutual solubility of the same components in the crystalline state. Well known examples are the high solubility of NaCl or sugar in water and the low solubility of NaCl or sugar in ice. As a consequence in multi-phase nano-glasses, one will be able to obtain glassy solid solutions of components that are immiscible in the crystalline state.

In addition to the multi-phase metallic nano-glasses discussed so far, a wide spectrum of nano-glasses is predicted to exist e.g. with different types

of chemical bonds such as nano-glasses of a covalent and a metallic component, nano-glasses with different volume fraction of the components etc. None of these multi-phase nano-glasses has yet been explored.

Multi-phase nano-glasses produced by phase separation have been studied in alloy systems that exhibit negative enthalpies of mixing in the liquid phase. Examples of such systems are Ag-Ni (He *et al*. 2001), Cu-Nb (He *et al*. 2001), Ag-Cu (Albe *et al*. 2012; Michaelson *et al*. 1997; Duwez *et al*. 1960), Ag-Fe (Ma 2003), Ag-Gd (Hauser 1975), Cu-Ta (Nastasi *et al*. 1985) and Cu-W (Nastasi *et al*. 1985).

(b) Multi-phase Nano-glasses:Nano-porous Materials

In this section, we discuss multi-phase nano-glasses that consist of the following two phases: one phase is anano-porous (mostly crystalline) material, the other phase has a nanometer-sized amorphous structure either in the form of a liquid, a glass or a gas.

The underlying concept of these materials with liquid, glass or gas filled ligaments is that the properties of solid/liquid, solid/glass or solid/gasinterfaces can be tuned by variation of the state variable in the surrounding medium, for instance, the electric or chemical potential of the electrolyte in the ligaments (Weissmueller *et al*. 2003). Fig. 23 is a schematic illustration of the induced electric charge

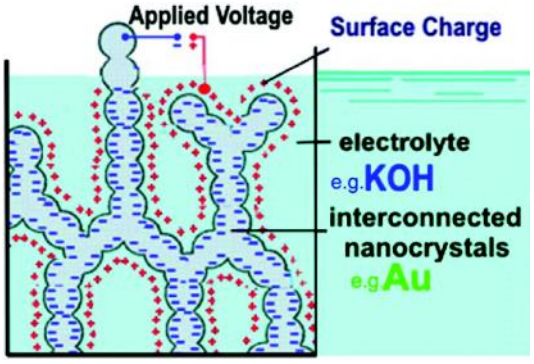

Fig. 23: Generation of an electrically charged surface in a nano-porous metal (e.g. Au) if it is immersed into a suitable electrolyte (here KOH) and if a voltage is applied between the metal and the electrolyte so that a double-layer is formed at the surface of the nano-porous metal (Weissmueller 2003)

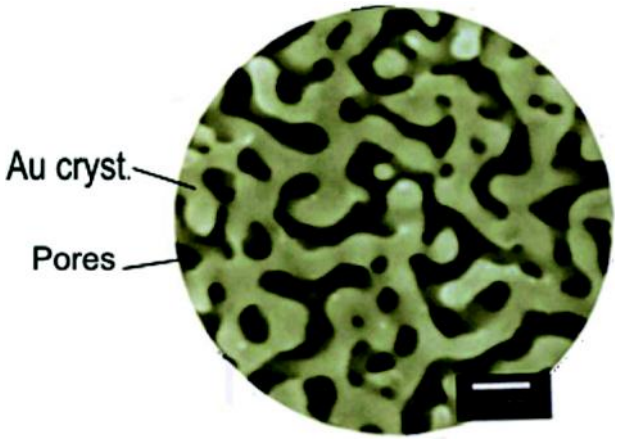

Fig. 24: Electron micrograph of nano-porous Au (Nagendran 2004)

in the surface region of a nano-porous metal due to an electrochemical double layer formed at the interface between the electrolyte and thenano-porous metallic material. By means of this induced electric charge, all properties of the nano-porous metal that depend on its electronic structure may be tuned. Due to the high density of ligaments ($\sim 10^{15}$ mm^{-3}) the nano-porous material reacts as a whole and hence behaves like a micro-structurally homogeneous solid of macroscopic dimensions with tunable mechanical, electrical, magnetic etc. properties.

(c) Surface Stress Driven Actuation

So far electric charge driven actuation has been studied in nano-porous metals (Weissmueller 2003; Kramer 2004) carbon nanotube materials (Baughman *et al*. 1999), vanadium oxide nano-fibers (Gu *et al*.)

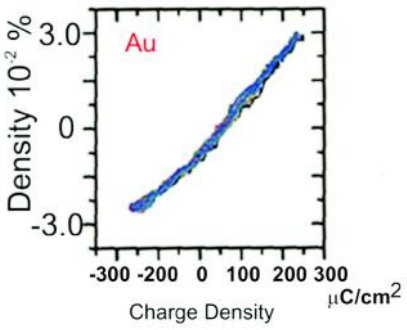

Fig. 25: Variation of the density of nano-porous Au vs. the electric charge density. The density variation was computed on the basis of the measured strain when the charge was applied. The scan rates were 1 mV/s (black), 0.8 mV/s (red) 0.4 mV/s (green), 0.2 mV/s (blue) (Weissmueller 2003; Kramer 2004)

and conducting polymers (Baughman 1996). In nano-porous metallic materials, strain amplitudes of up to 0.1 (i.e. strains comparable to those of commercial piezo-ceramics) were reported (Weissmueller 2003; Kramer 2004). Figure 24 shows the scanning electron micrograph of a surface of nano-porous Au. If samples of this kind were immersed in one the following aqueous electrolytes: H_2SO_4 (0.5 M), $HClO_4$ (1 M) or KOH (1 M) and if an electro-chemical potential was applied between the Au and one of the electrolytes, the resulting strain varied almost linearly if it was plotted against the surface charge density (Fig. 25).

In addition to nano-porous metals, charge-driven reversible actuation of carbon nanotubes has been studied for carbon single-walled-nanotube sheets (SWNT) (Baughman 1996) as electrolyte-filled electrodes of a super-capacitor. If the applied voltage was varied, an electronic charge was injected into the SWNT electrode. This charge injection results in dimensional changes of the carbon nanotubes.

(d) Surface Chemistry Driven Actuation

Although actuation in biological systems, e.g. of muscles, is exclusively powered by chemical energy, this concept has not been realized in man-made actuator technologies for a long time.

However, in recent years, man-made surface-chemistry driven actuators have been reported that are based on metallic materials as well as on electrically conducting polymers such as polyaniline and polypyrrole. These materials actuate by electrochemically inserting solvated dopant ions into a conducting-polymer electrode and may produce strains (up to 26%) matching those of natural muscles (Bienar *et al*. 2009; Sagmeister *et al*. 2006). The second type of surface-chemistry driven actuators are based on dielectric elastomers which constitute capacitors. Actuation results from the attraction between charges on opposite capacitor electrodes. A third type of artificial muscles uses the volume change of an electrolyte and electrostatic repulsion (Dasgupta *et al*. 2008; Drings *et al*. 2006). These actuators (Ghosh *et al*. 2006) consist of two metallic nanoparticle electrodes that are both filled with a solid electrolyte and separated by this electrolyte. Tensile strains of up to 40 % have been produced (Mitsudome *et al*. 2008).

(e) Density Driven Actuation

Recently, thermally, electro-thermally and photo-thermally powered torsional and tensile actuation of hybrid carbon nanotube yarn has been demonstrated (Lima *et al*. 2012) by means of infiltrated (mostly with wax) twist-spun carbon nanotubes. They are electrolyte-free and provide high force, large stroke torsional and tensile actuation with tensile contractions of 3 % with up to 1200 cycles/minute. If the wax was molten, its thermal expansion increased the diameter of the infiltrated nanotubes and – as a consequence – the tubes contracted with a force that was up to 104 times the weight of the actuator.

(f) Electric Conductivity

Already in 1973 a first attempt to vary the resistivity of a metal electrochemically was performed by Anderson and Hansen (Anderson *et al*. 1973; Anderson and Hansen 1973). These authors immersed a thin gold film in an aqueous Na_2SO_4 solution. The experiment, however, yielded only a small change of about 0,4 % of resistivity.

In recent years, the availability of nano-porous materials opened the way to new studies in this area (Sagmeister *et al*. 2006; Bongfiglioli *et al*. 1956; Tucceri *et al*. 1983; Tucceri 2004; Bansal *et al*. 2007; Weisheit *et al*. 2007; Mishra *et al*. 2007). In fact, more recent measurements of the surface-charge driven resistivity variation were performed for Au and Pt (Sagmeister *et al*. 2006; Mishra *et al*. 2008) using electrochemical cells. The observed variation of the conductivity in nano-porous Au was found to depend linearly on the electric charge density. This result suggests that it is the electric charge rather than chemical effects – such as uptake of hydrogen – that causes the observed variations of the resistivity/ conductivity. This conclusion is further supported by cyclic voltagrams of the porous nano-crystalline Pt specimen as well as by literature data (Haman and

Vielsteich 1988). The interpretation of the experimental results mentioned so far in terms of the charge-induced variation of the electrical resistance of a metal is furthermore supported by studies of the resistance variation of graphite fibers used in super-capacitors as well as by studies using nanometer-sized ITO layers (Dasgupta 2006). Because of the much lower carrier concentrations in graphite and in ITO, a substantially higher resistance variation occurs under identical charging conditions in comparison to e. g. nano-porous Pt or Au (Sagmeister *et al*. 2006; Mishra *et al*. 2008). In fact, the resistivity of a 3.6 nm thick ITO layer with a carrier density of about 10^{20} cm^{-3} varied by about 300% if a voltage of about 1 V was applied. This remarkable resistivity change could be understood in terms of the variation of both, the charge carrier density and their mobility.

(g) Superconductivity

One approach to modify the electric properties of superconductors is by introducing impurities into the crystal lattice e. g. by chemical doping. An alternative approach involves tuning the density of charge carriers by applying an external electric field. Recently superconductivity has been induced by means of this approach in strontium titanate, $SrTiO_3$. (Ueno *et al*. 2008). In fact, $SrTiO_3$ was doped by using $SrTiO_3$ as one of the electrodes in an electrochemical cell as is shown in Fig 26. When immersed in an organic electrolyte with a platinum wire electrode, the resistance of the $SrTiO_3$ declined sharply at voltages above 2.5 V. Upon reducing the temperature to 0.4 K, the normally insulating $SrTiO_3$ became a superconductor (Fig. 26). Examination of the $SrTiO_3$ surface revealed that this transition is due to the accumulation of positive electric charge near the surface rather than to electrochemical reactions.

(h) Ferromagnetic Properties

3d-transition metals are known to have partially filled d-bands in the metallic state. For convenience, this is often expressed by interpreting the magnetization to arise from holes in the 3d band. Hence, if Ni is charged (by an applied voltage) with excess electrons, these excess electrons may fill the unoccupied 3d states of Ni. Just as in the case of e.g. Ni-Cu alloys, the changing population of the unoccupied 3d states may be expected to modify the magnetic properties of Ni. Indeed, recent measurements support this idea (Figs. 27 and 28). In fact, the magnetic moment of a nano-prous $Pd_{67}Ni_{33}$ alloy, the pores of which were filled with an electrolyte (KOH, 1N), the magnetic moment of the Pd-Ni alloy was seen to vary by almost 40% if a potential of ± 0.5 V was applied between the electrolyte and the $Pd_{67}Ni_{33}$ alloy (Gleiter *et al*. 2003). A comparable variation of the magnetic moment was noted (Fig. 27) in nano-crystalline Pd if the electronic structure was varied by applying an external voltage (Drings *et al*. 2006). In fact, the variation of the magnetic properties by means of tuning the electron density may even open the way to synthesize materials in which ferromagnetism may be "switched on and off".

Direct evidence for the variation of the electron density in the d-band as a function of the applied voltage has been obtained by means of X-ray absorption studies of nanometer-sized Pt-25 at% Ru crystallites (McBeen and Mukherjee 1995). The strong increase and decreases in optical absorption (Fig. 28) which occurred on the two flanks of the 380 nm plasmon band of the silver particles indicate that the band is shifted towards shorter wavelengths upon electron (and to longer wavelengths upon positive hole) injection.

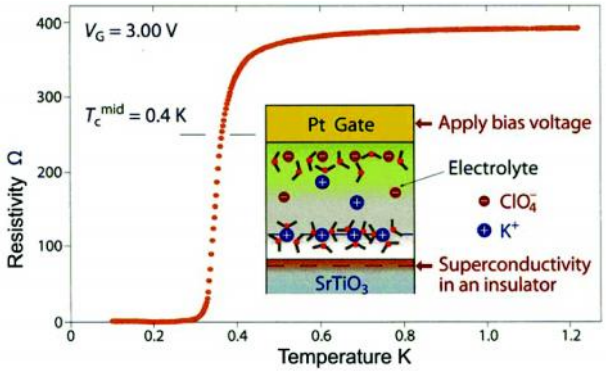

Fig. 26: Abrupt disappearance of the resistivity (W) of $SrTiO_3$ as the temperature drops to 0.4 K at a gate voltage (V_G) of 3 V. The inset shows a schematic diagram of the structure of the electric double-layer that was used to modify the charge carrier density in the $SrTiO_3$ (Ueno *et al*. 2008)

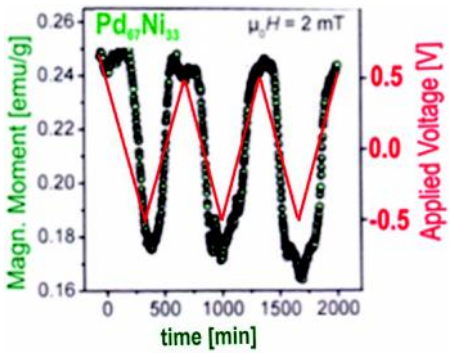

Fig. 27a: Variation of the magnetic moment of nano-porous $Pd_{67}Ni_{33}$ as a function of the electric charge induced by an externally applied voltage between the electrolyte (KOH) and the nano-porous material (cf. Figs. 23 and 24). The red line indicates the variation of the applied voltage. The externally applied magnetic field of 2mT was constant during the measurement (Gleiter *et al*. 2003)

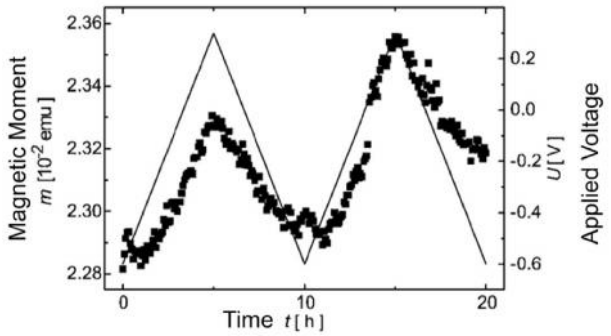

Fig. 27b: Magnetic moment (m) of nano-crystalline Pd vs. time (t) upon in situ charging with a voltage (U, solid line) (Drings *et al*. 2006)

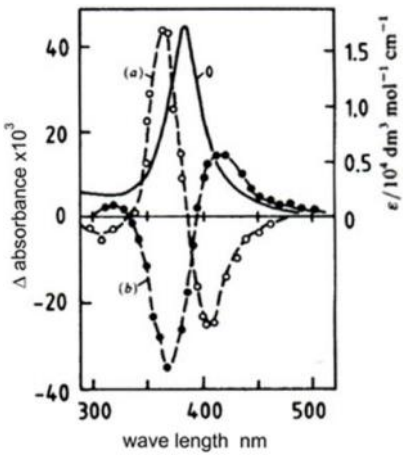

Fig. 28: Surface plasmon absorption band of a 1 x 10^{-1}mol m^{-1} silver sol consisting of an aqueous suspension of 2 nm sized Ag crystallites. The variation of the absorbance (a) after electron injection and (b) after hole injection into the silver crystallites by free radicals is shown. O is the absorbance of electrically neutral silver crystallites (McBeen and Mukherjee 1995)

7. Conclusions

(a) Outlook

This paper has been started by considering the role of materials in the history of mankind. Hence it seems appropriate to close the paper by considering the conceivable implications of the development reported here for the future of mankind.

In the past, the understanding and utilization of materials such as metals, semiconductors, ceramics etc. resulted in specific periods of the development of mankind. In fact, the names of some of these periods were selected according to the names of these materials such as the ironage, the bronze age etc. The majority of these materials were *crystalline materials.* The main reason for the preference of crystalline materials was the fact that one can control their properties by modifying their defect microstructure and/or their chemical microstructure. In fact,utilizing the controlled variation of the properties for each group of these crystalline materials opened the way tonumerous new technologies.

Today, we seem to be in a comparable situation for materials with *non-crystalline structures.* In fact, nano-glasses seem to open the way to new kinds of non-crystalline materials with controllable defect microstructures and/or chemical microstructures resulting in non-crystalline materials with new atomic and new electronic structures and, hence,new properties(in comparison to the properties of the glasses available today that are produced by quenching the melt). Hence, by analogy to the technological developments in the past based on crystalline materials, nano-glasses may permit thedevelopmentof a large variety of newtechnologies that are not possible with the glassy materials we have today.

A prerequisite for a development of this kind is, however, that one succeeds in developing economic methods for producing large quantities of nano-glasses with well controlled microstructures.

8. Acknowledgments

The author gratefully acknowledges the numerous contributions from his colleagues all over the world, in particular from Professors/Drs. Albe, Birringer, Hahn, Fang, Feng, Jiang, Na, Schimmel, Sopu, Vainio, Weissmueller, Witte. The contributions of these colleagues as well as from numerous others opened the way to the studies summarized in this paper.

References

Albe K, Ritter Y and Sopu D E-MRS Fall Meeting 2011, Symposium E *Mechanics of Materials* **3** (2012) **9**1-9

Anderson W J and Hansen W N *J Electroanal Chem* **43** (1973) 329-335

Anderson W J and Hansen W N *Electroanal Chem Interfacial Electrochem* **47** (1973) 229-336

Arnold M, Cavalcanti-Adam E A, Glass R, Blümmel J, Eck W, Kantlehner M, Kessler H and Spatz J P *Chem Phys Chem* **5** (2004) 383-388

Banerjee R, Puthucode A, Bose S and Ayyub P *Appl Phys Lett* **90** (2007) 021904

Baughman R H, Cui C, Zakhidov A, Iqbal Z, Barisci J N, Spinks G, Wallace G, Mazzoldi A, de Rossi D, Ruizler A G, Jaschinski O, Roth S and Kertesz M *Science* **284** (1999) 1340-1346

Bansal C, Sarkar S, Mishra A K, Abraham T, Lemier C and Hahn H *Scripta Mat* **56** (2007) 705-710

Drings H, Viswanath R, Kramer D, Lemier C, Weissmueller J and Wuerschum R *Appl Phys Lett* **88** (2006) 253103-1/3

Baughman R H *Synth Met* **78** (1996) 339-342

Biener J, Wittstock A, Zepeda-Ruiz L, Biener M M, Kramer D, Viswanath R N, Weissmueller J, Baeumer M, Hamza A V *Nature Mater* **8** (2009) 47

Bongfiglioli G Coen E and Malvano R *Rev Phys* **101** (1956) 1281-1286

Cao Q P, Liu J W, YangK J, Xu F, YaoZ Q, Minkow A, Fecht H J, Ivanisenko J, Chen L Y, Wang X D, Qu S X and Jiang J Z (2010) *Acta Mater* **58** (2006) 1276-1292

Chauhan B P S, Sarkar A, Chauhan M and Roka A *Appl Organometal Chem* **23** (2009) 385-391

Chen N, Frank R, Asao N, Louzguine-Luzgin D V, Sharma P, Wang J Q, Xie G Q, Ishikawa Y, Hatakeyama N, Lin Y C, Esashi M, Yamamoto Y and Inoue A *Acta Materialia* **59** (2011) 6433-6440

Cheng Y Q, Cao A J, Sheng H W and Ma E *Acta Mater* **56**(18) (2008) 5263-5275

Chen N, Shi X, Witte R, Nakayama K S, Okamura A, Louzguine-Luzgin D V, Wu H, Takeuchi A, Hahn H, Esashi M, Gleiter H and Inoue A (2013) *J Mater Chem B*, **1** (2013 2568-2574

Chen N, Hahn H and Gleiter H (unpublished)

Chokshi A, Feng T, Witte R, Hahn H and Gleiter H (unpublished)

Dasgupta S, Gottschalk S, Kruk R and Hahn H *Nanotechnology* **19** (2008) 435203

Dasgupta S *Phys Rev B* **80** (2009) 085425

Denmark S E, Sweis R F *In*: Metal-Catalyzed Cross-Coupling Reactions, de MeijereA, DiederichF, (2004) editors, Wiley-VCH, Weinheim

Denmark S E and Wehrli D *Org Lett* **2** (2000) 565-566

Drings H, Viswanath R N, Kramer D, Lemier C, Weissmueller J and Wuerschum R *Appl Phys Lett* **88** (2006) 253103

Duwez P, Willens R H and Clement W *J Appl Phys* **31** (1960) 1136-1141

Fang J X, Vainio U, Puff W, Wuerschum R, Wang X L, Wang D, Ghafari M, Jiang F, Sun J, Hahn H and Gleiter H *Nano Letters* **12** (2012) 458-463

Fang J X, Wang X L, Wang D, Hahn H and Gleiter H (Submitted to *Advanced Materials* 2013)

Feng T, Witte, Hahn H and Gleiter H (unpublished work)

Franke O, Hodges A, Feng T, Witte R, Hahn H and Gleiter H (unpublished)

Ghafari M (unpublished)

Ghafari M, Hahn H, Gleiter H, Sakurai Y, Itou M, Kamali S *Appl Phys Letters* **100** (2012) 133111

Ghafari M, Hahn H, Gleiter H, Sakurai Y, Itou M and Kamali S *Appl Phys Lett* **101** (2012) 234104-1

Ghafari M, Kohara S, Hahn H, Gleiter H, Feng T, Witte R and Kamali S *Appl Phys Lett* **100** (2012) 133111-1

Ghosh S, Lemier C and Weissmueller J *IEEE Trans Magn* **42** (2006) 3617-3521

Gleiter H *J Appl Cryst* **24** (1991) 79-84

Gleiter H *Acta Materialia* **56** (2008) 5875-5893

Gleiter H Nordrhein-Westfälische Akademie der Wissenschaften, F Schoeningh-Verlag *Vorträge Nr* **463** (2003) 47-88

Gu G, Schmid M, Chiu P W, Minett A, Fraysse J, Kim G and Baughman R H(v) *Nature mater* **315** 316-319

Hamam C H and Vielstich W (1988) Elektrochemie, Wiley Publ. VHC Weinheim, Germany p. 266

Hauser J *J Phys Rev B* **12** (1975) 5160-5168

He J H, Sheng H W, Schilling P J, Chien C-L and Ma E *Phys Rev Lett* **86** (2001) 2826

Kramer D, Viswanath R N and Weissmueller J *Nano Lett* **4** (2004) 793-796

He J H, Sheng H W and Ma E *Appl Phys Lett* **78** (2001) 1343

Hirabayashi K, Nishihara Y, Mori A and Hiyama T *Tetrahedon Lett* **39** (1998) 7893

Hirabayashi K, Kawashima J, Nishihara Y, Mori A and Hiyama T *Org Lett* **1** (1999) 299

Hofmann D C, Suh J Y, Wiest A, Duan G, Lind M L, Demetriou M D and Johnson W L *Nature* **451** (2008) 1085-1090

Huang J, Graeter S V, Corbellini F, Rinck S, Bock E, Kemkemer R, Kessler H, Ding J and Spatz J P *Nano Letters* **9** (2009) 1111-1116

Jing J, Kramer A, Birringer R, Gleiter H and Gonser U J *Non-Cryst Solids* **113** (1989) 167-173

Kelly A and Nicholson R B *Prog Mater Sci* **10** (1963) 1

Kuhn A, Wilkening M and Heitjans P *Solid State Ionics* **180** (2009) 302-307

Kuhn A, Tobschall E and Heitjans P *Z Phys Chem* **223** (2009) 1359-1377

Lee J C, Park K W, Kim K H, Fleury E, Lee B J, Wakeda M and Shibutani Y *J Mater Res* **22** (2007) 3087-3089

Li J, Wang Z L and Hufnagel T C *Phys Rev B* **65** (2002) 144201

Lima M D, Li Na, Andrade M., Fang S., Oh J., Spinks G, Kozlov M, Haines C, Suh D, Foroughi J, Kim S, Chen Y, Ware T, Shin M, Machado L, Fonseca A, Madden L, Voit W, Galvao D and Baughman R H *Science* **338** (2012) 928-932

Linde R K *J Appl Phys* **37** (1966) 934-941

Liu J W, Cao Q P, Chen L Y, Wang X D and Jiang J Z *Acta Mater* **58** (2010) 4827-4831

Ma E *Scr Mater* **4** (2003) **9**941-944

McBeen J and Mukherjee S *J Electrochem Soc* **142** (1995) 3399-3402

Mendelev M I, Sordelet D J and Kramer M J *J Appl Phys* **102** (2007) 043501

Michaelson C, Gente C and Bormann R *J Appl Phys* **81** (1997) 6024-6027

Mitsudome T, Arita S, Mori H, Mizugaki T, Jitsukawa K and Kaneda K *Angew Chem Int Ed* **47** (2008) 7938-7940

Mitsudome T, Noujima A, Mizugaki T, Jitsikawa K and Kaneda K *Chem Commun* **35** (2009) 5302-5304

Mitsudome T, Arita S, Mori H, Mizguki T, JitsukawaK, Kaneda K *Angew Chem Int Ed* **47** (2008) 7938, 1-4

Mishra A K, Bansal C and Hahn H *J Appl Phys* **103** (2008) 094308

Morrison M L, Buchanan R A, Peker A, Laiw P K, Horton J A *J Non-cryst Solids* **353** (2007) 2115-2116

Murugavel R, Walawalkar M G, Dan M, Roesky M WRao C N R *Acc Chem Res* **37** (2004) 763-771

Nagendran S *Chem Rev* **104** (2004) 5847-5852

Nastasi M, Saris F W, Hung L S and Mayer J W *J Appl Phys* **58** (1985) 3052-3058

Oak J J, Louzguine-Luzgin D V and Inoue A *J Mater Res* **22** (2007) 1346

Park B J, Chang H J, Kim D H, Kim W T, Chattopadhyay K, Abinandanan T A and Bhattacharyya S *Phys Rev Lett* **96** (2006) 245503

Qin F X, Wang X M, Zhu S L, Kawashima A, Asami K and Inoue A *Mater Trans* **48** (2007) 515-519-522

Ritter, Sopu D, Gleiter H and Albe K *Acta Materialia* **59** (2011) 6588-6593

Sagmeister M, Brossmann U, Landgraf S and Wuerschum R *Phys Rev Lett* **96** (2006) 156601

Sagmeister M, Brossmann U L and Graf S and Wuerschum R *Phys Rev Lett* **96** (2006) 156601

Sakurai Y, Tanak Y, Ohata T, Watanabe Y, Nanao S, Ushigami Y, Iwazumi T, Kawata H and Shiotani N *J Phys* **6** (1994) 9469

Sakai N *Materials Science Forum* **105-110** (1992) 431-438

Selhuber-Unkel C, Erdmann T, López-García M, Kessler H, Schwarz U S and Spatz J P*Biophysical Journal* **98** (2010) 543-551

Shao H, Yu Y, Shi B, Yu Ch, Hahn H, Gleiter H and Li J J *Alloys and Compounds* **548** (2012) 77-81

Sond S X, Jang J S C, Huang J C and Nieh T G *Intermetallics* **18** (2010) 702-709

Sopu D, Albe K, Ritter Y and Gleiter H *Appl Phys Lett* **94** (2009) 191911/1-3

Sopu D, Ritter Y, Gleiter H and Albe K *Phys Rev B* **83** (2011) 100202/1-4

Takayama S *Mater Sci Enging* **38** (1979) 41-44

Tucceri R I, Molina F and Posadas D *Anal Asoc Quim Arg* **71** (1983) 241-246

Tucceri R I *Surf Sci Rep* **56** (2004) 85-96

Ueno K, Nakamura S, Shimotani H, Ohtoma A, Kimura N,

Nojima T, Aoki H, Iwasa Y and Kawasaki M *Nature Materials* **7** (2008) 855-858

Wang J G, Zhao D Q, Pan M X, Shek C H and Wang W H *Appl Phys Lett* **94** (2009) 031904-3

Weissmueller J, Schubert P, Franz H, Birringer R and Gleiter H (1991) Proc VII Natl Conf on the Physics of Non-Crystall. Solids Cambridge, England August 4-9

Weissmueller J, Newman R C, Jin H-J, Hodge A M and Kysar J W *MRS Bulletin* **34** (2009) 577-591

Weissmueller J, Viswanath R N, Kramer D, Zimmer P, Wuerschum R and Gleiter H *Science* **300** (2003) 312-315

Weisheit M, Faehler S, Marty A, Souche Y, Poinsignon C and Givord D *Science* **19** (2007) 5810-5818

Wilkening M and Heitjans P *J Phys Condens Matter* **18** (2006) 9849-9851

Witte R, Feng T, Fang J X, Fischer A, Ghafarai M, Brand R A, Wang D, Hahn H and Gleiter H *Appl Phys Lett* **103** (2013) 073106

Wuerschum R, Reimann K and Farber P *Defect Diffus Forum* **1483** (1997) 143-147

Yang B and Nieh T G *Acta Mater* **55** (2007) 295-300

Zukoeski E, Cooper M J, Timms D N, Armstrong R, Itoh F, Sakurai H, Tanaka Y, Ito M, Kawata H and Bateson R *J Phys Soc Jap* **63** (1994) 3838-3841.